evaluation. J Chem Soc Jpn 1998;106:709-714.

29. Brandrup J, Immergut EH (eds), Polymer Handbook 3rd Edition, Wiley and Sons Inc., New York, 1989

30. Pluedemann EP (ed), Silane coupling agent, Plenum Press, New York, 1991.

31. Mittal KL (ed), Silane and other coupling agents, VSP, Utrecht, 1992.

32. Okada M, Furukawa K, Serizawa T, Yanagisawa Y, Tanaka H, Kawai T, Furuzono T. Estimation of interfacial interaction strength between calcined hydroxyapatite nanocrystals and substrate surface, in preparation.

33. Kilpadi KL, Chang PL, Bellis SL. Hydroxylapatite binds more serum proteins, purified integrins, and osteoblast precursor cells than titanium or steel. J Biomed Mater Res 2001;57:258-267.

34. Kawasaki T, Niikura M, Kobayashi Y. Fundamental study of hydroxyapatite high-performance liquid chromatography III. Direct experimental confirmation of the existence of two types of adsorbing surface on the hydroxyapatite crystal. J Chromatogr A 1990;515:125-148.

35. Deligianni D D, Katsala N D, Koutsoukos P G, Missirlis Y F. Effect of surface roughness of hydroxyapatite on human bone marrow cell adhesion, proliferation, differentiation and detachment strength. Biomaterials 2001; 22: 87-96.

36. Okano T, Uruno M, Sugiyama N, Shimada M, Shinohara I, Kataoka K, Sakurai Y. Suppression of platelet activity on microdomain surfaces of 2-hydroxyethyl methacrylate-polyether block copolymers. J Biomed Mater Res 1986;20:1035-1047

37. Okano T, Kataoka K, Sakurai Y, Shimada M, Miyahara M, Akaike T, Shinohara I. Molecular design of block and graft copolymers having the ability to suppress platelet adhesion. Artif Organs 1981;5:468-470

38. Kannan S, Balamurugan A, Rajeswari S, Subbaiyan M. Metallic implants. An approach for long term applications in bone related defects. Corros Rev 2002;20:339-358.

39. Schnuch A, Geier J, Lessmann H, Uter W. Decrease in nickel sensitization in young patients--successful intervention through nickel exposure regulation? Results of IVDK, 1992-2001, Hautarzt 2003;54:626-632.

40. Köster R, Vieluf D, Kiehn M, Sommerauer M, Kahler J, Baldus S,Meinertz T, Hamm CW. Nickel and molybdenum contact allergies in patients with coronary in-stent restenosis. Lancet 2000;356:1895-1897.

Table 1 Atomic percentages of the surfaces of the stainless-steel substrates evaluated by X-ray photoelectron spectroscopy

	C	O	Si	S	Cr	Fe	Ni
Original	25.9	50.9	0.6	0.4	10.6	5.0	1.0
Silized	35.0	44.4	2.5	1.9	9.3	5.0	0.6
Poly(MPTS)-Grafted	68.2	27.0	4.8	-	-	-	-

Table 1 Okada *et al.*

Figure captions

Fig. 1 Schematic process diagram of HAp nanocrystal coating for stainless-steel substrate through covalent linkage.

Fig. 2 SEM photographs of (a) spherical and (b) rod-shaped HAp nanocrystals prepared by wet chemical process followed by calcination at 800°C with anti-sintering agent.

Fig. 3 ATR FT-IR spectra of (a) poly(γ-methacryloxypropyl trimethoxysilane) prepared by solution polymerization and (b) the surface of stainless-steel substrate after the graft polymerization.

Fig. 4 SEM photographs of the surfaces of (a) the original stainless-steel substrate and (b–d) the substrates after the HAp nanocrystal coating followed by ultrasonic washing. Poly(MPTS)-grafting: (a, b) nonexistence; (c, d) existence. HAp nanocrystals: (b, c) spherical; (d) rod-shaped.

Fig. 5 SEM photographs of HUVEC adhering on (a) the original, (b) tissue culture polystyrene (TCPS), (c) spherical HAp-coated, and (d) rod-shaped HAp-coated stainless-steel substrates after incubation in 24-well multiplates (8×10^4 cells/cm^2) at 37°C for 24 h.

Fig. 6 Number of HUVEC adhering on (a) the original, (b) spherical HAp-coated, and (c) rod-like HAp-coated stainless-steel substrates after incubation in 24-well multiplates (8×10^4 cells/cm^2) at 37°C for 24 h. The number was normalized by the number of HUVEC that adhered on TCPS.

Fig. 7 Type 316L stainless-steel stent (a) before and (b) after coating with rod-shaped HAp nanocrystals, and (c) SEM photograph of the surface of the HAp-coated stent.

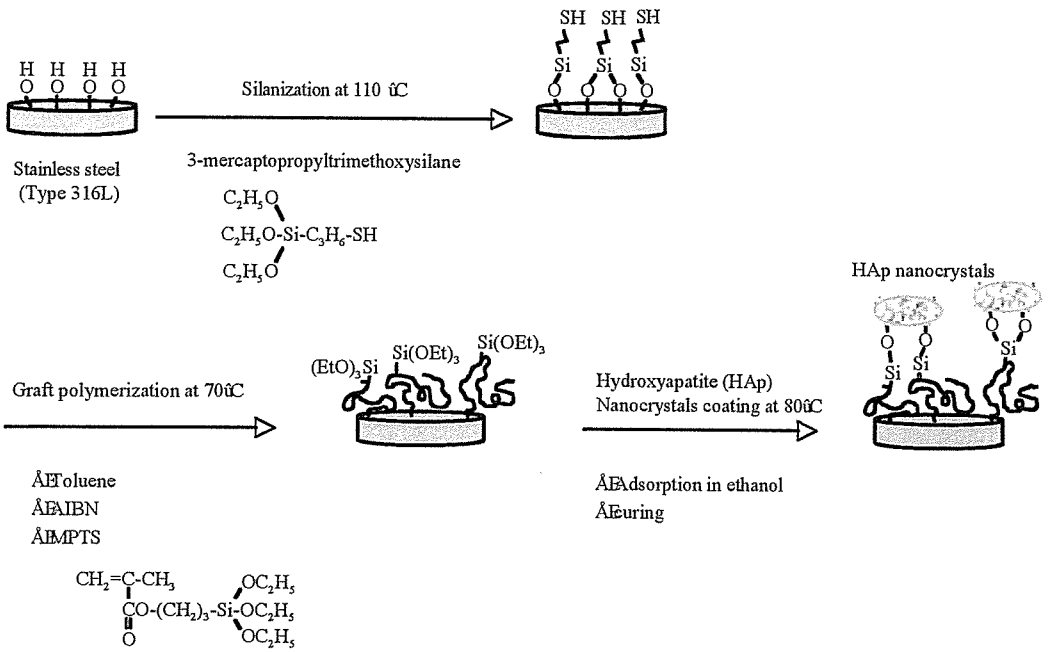

Fig. 1 Schematic process diagram of HAp nanocrystal coating for stainless-steel substrate through covalent linkage.

Fig. 1 Okada *et al.*

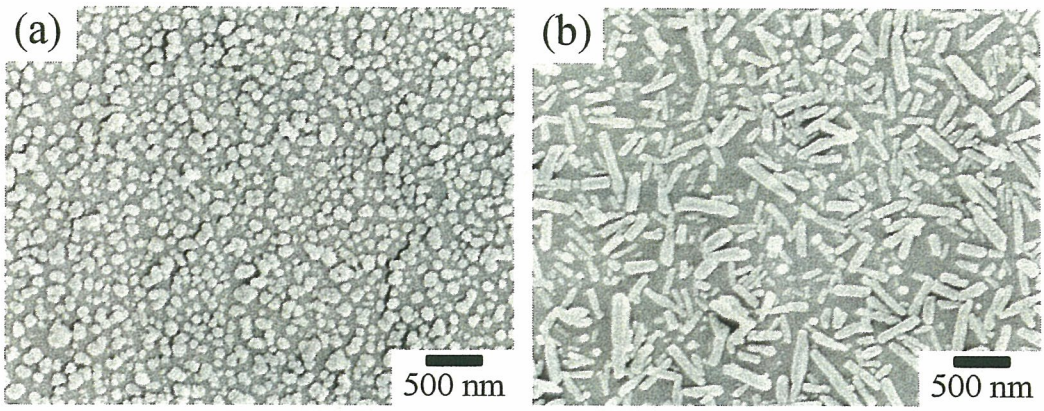

Fig. 2 SEM photographs of (a) spherical and (b) rod-shaped HAp nanocrystals prepared by wet chemical process followed by calcination at 800°C with anti-sintering agent.

Fig. 2 Okada *et al.*

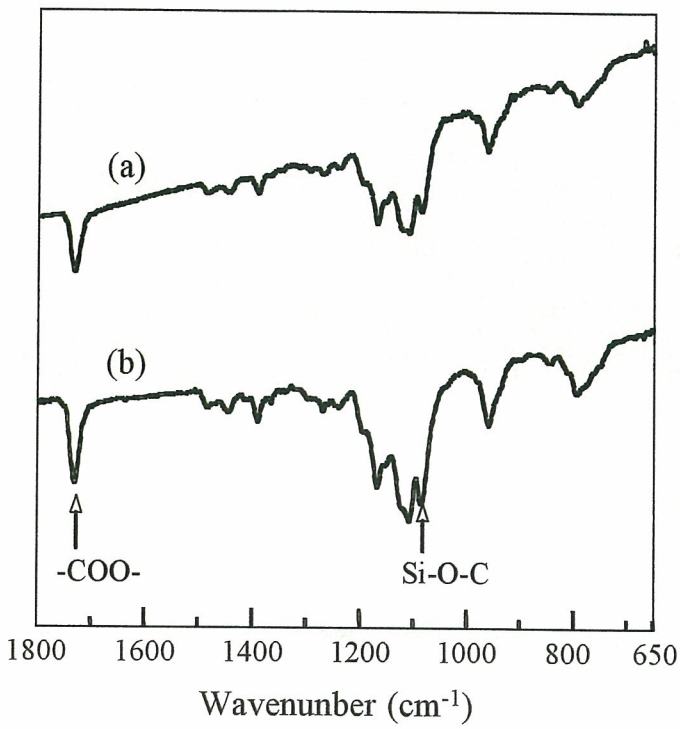

Fig. 3 ATR FT-IR spectra of (a) poly(γ-methacryloxypropyl trimethoxysilane) prepared by solution polymerization and (b) the surface of stainless-steel substrate after the graft polymerization.

Fig. 3 Okada *et al.*

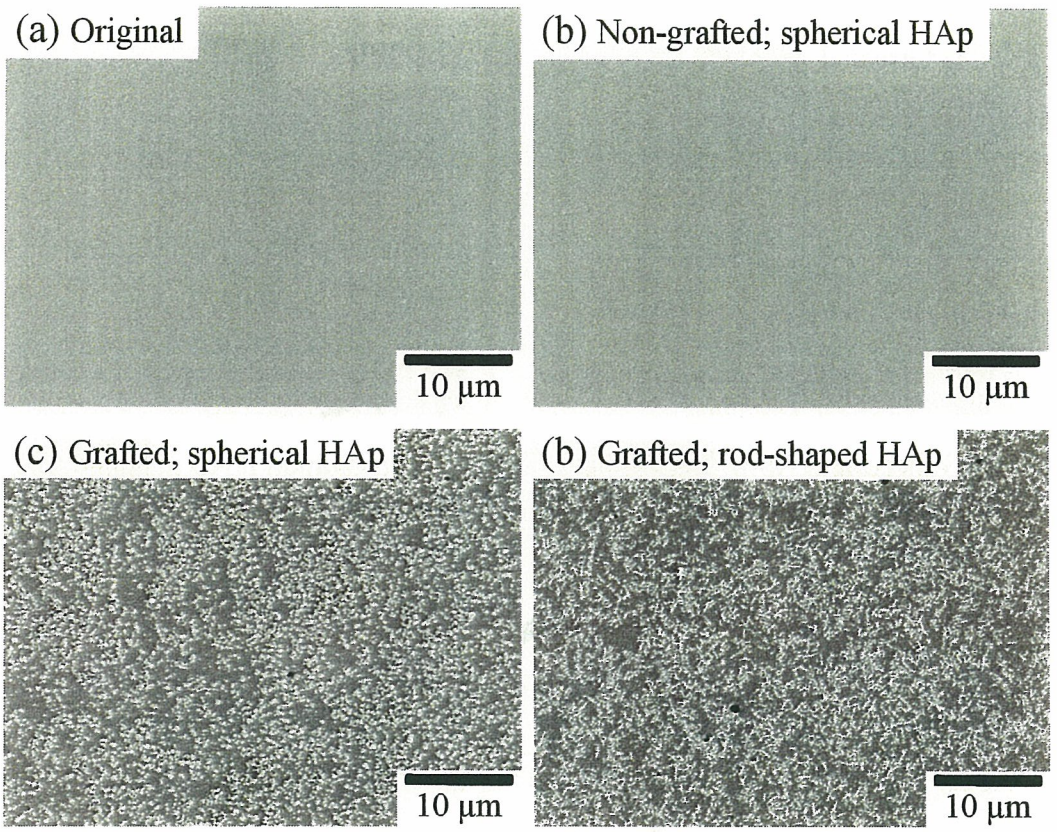

Fig. 4 SEM photographs of the surfaces of (a) the original stainless-steel substrate and (b–d) the substrates after the HAp nanocrystal coating followed by ultrasonic washing. Poly(MPTS)-grafting: (a, b) nonexistence; (c, d) existence. HAp nanocrystals: (b, c) spherical; (d) rod-shaped.

Fig. 4 Okada *et al.*

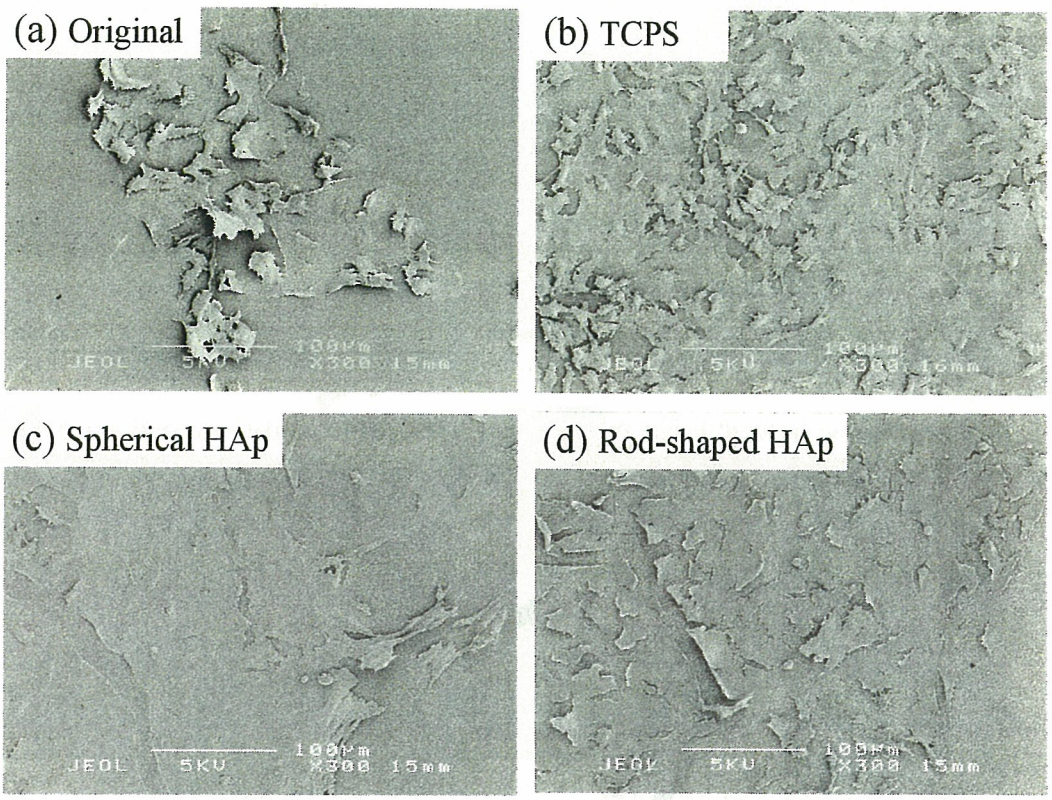

Fig. 5 SEM photographs of HUVEC adhering on (a) the original, (b) tissue culture polystyrene (TCPS), (c) spherical HAp-coated, and (d) rod-shaped HAp-coated stainless-steel substrates after incubation in 24-well multiplates (8×10^4 cells/cm^2) at 37°C for 24 h.

Fig. 5 Okada *et al.*

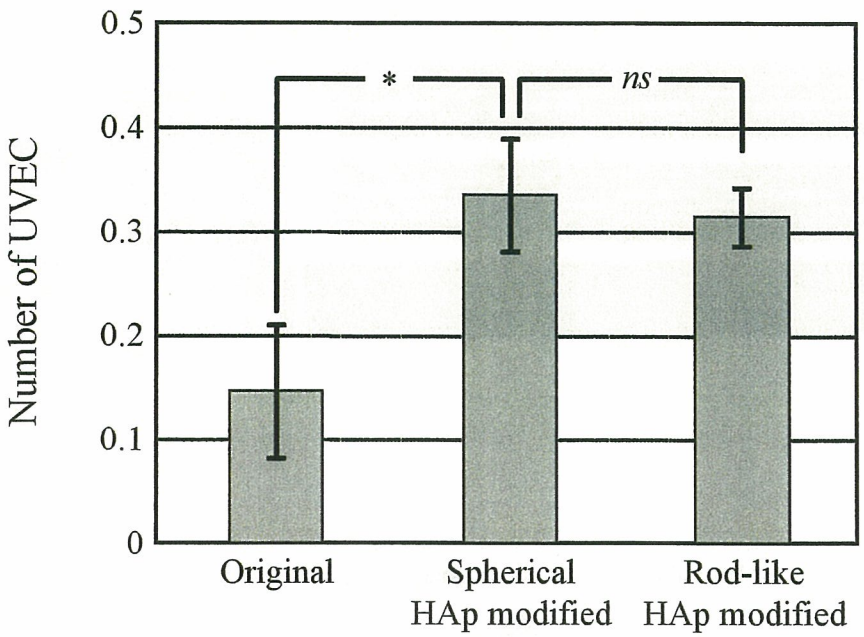

Fig. 6 Number of HUVEC adhering on (a) the original, (b) spherical HAp-coated, and (c) rod-like HAp-coated stainless-steel substrates after incubation in 24-well multiplates (8×10^4 cells/cm^2) at 37°C for 24 h. The number was normalized by the number of HUVEC that adhered on TCPS.

Fig. 6 Okada *et al.*

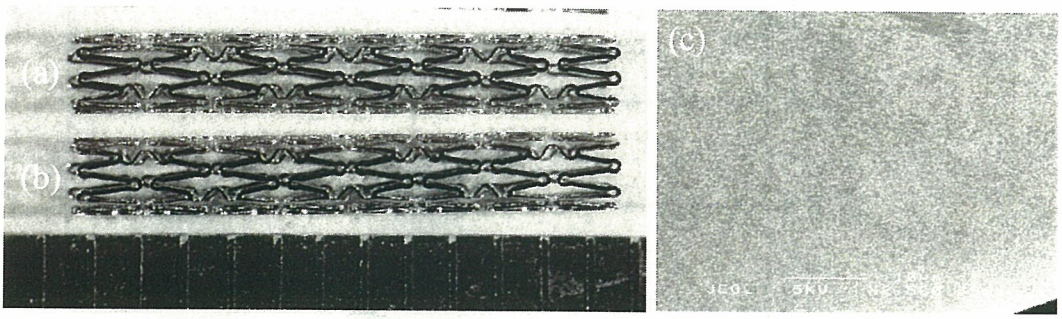

Fig. 7 Type 316L stainless-steel stent (a) before and (b) after coating with rod-shaped HAp nanocrystals, and (c) SEM photograph of the surface of the HAp-coated stent.

Fig. 7 Okada *et al.*